

## Antiskyrmions in Ferroelectric Barium Titanate

Mauro A. P. Gonçalves<sup>1</sup>, Marek Paściak<sup>1</sup>, and Jiří Hlinka<sup>1\*</sup>

*Institute of Physics of the Czech Academy of Sciences, Prague 182 21, Czech Republic*

 (Received 12 September 2023; revised 16 May 2024; accepted 21 June 2024; published 9 August 2024)

Typical magnetic skyrmion is a string of inverted magnetization within a ferromagnet, protected by a sleeve of a vortexlike spin texture, such that its cross-section carries an integer topological charge. Some magnets form antiskyrmions, the antiparticle strings which carry an opposite topological charge. Here we demonstrate that topologically equivalent but purely electric antiskyrmion can exist in a ferroelectric material as well. In particular, our computer experiments reveal that the archetype ferroelectric, barium titanate, can host antiskyrmions at zero field. The polarization pattern around their cores reminds ring windings of decorative knots rather than the typical magnetic antiskyrmion texture. We show that the antiskyrmion of barium titanate has just 2–3 nm in diameter, a hexagonal cross section, and an exotic topological charge with doubled magnitude and opposite sign when compared to the standard skyrmion string.

DOI: [10.1103/PhysRevLett.133.066802](https://doi.org/10.1103/PhysRevLett.133.066802)

Discovery of topologically stable nanoscale swirling defects of magnetization textures in chiral ferromagnets [1,2], termed as magnetic skyrmions, has opened amazing perspectives for information storage technology [3] as well as a vast arena for studies of intriguing new physics phenomena [4,5] like the topological Hall effect [6] and the skyrmion Hall effect [7–9]. It is now well understood that skyrmions and similar topological defects can be stabilized in many other, sometimes even achiral or centrosymmetric, magnets and antiferromagnets [10–15].

Geometrically analogous nanoscale swirling defects of electric polarization textures have been also observed in nonmagnetic ferroelectric materials [16]. They have been attracting attention due to their truly nanoscale size [16–18] and intriguing properties such as negative capacitance [19] or emergent chirality [20–23]. Experimental evidence of “electric” skyrmions (see Supplemental Material, note 1 [24]) in nanostructures consisting of nanoscale layers of ferroelectric  $\text{PbTiO}_3$  combined with paraelectric layers of  $\text{SrTiO}_3$  [16] pointed towards the basic role of the interface effects. These observations raised a question whether such electric skyrmions can be stable in the bulk of the ferroelectric material itself.

Natural candidate materials are those in which the electric polarization is expected to rotate gradually within the thickness of their domain walls. Figure 1(a) shows a plausible geometry of a columnar nanodomain in bulk

$\text{PbTiO}_3$ . The nanodomain, defined by the polarization parallel to  $z$  direction, is surrounded by a matrix of the opposite polarization. Computational study of Ref. [17] suggests that in  $\text{PbTiO}_3$ , an in-plane polarization develops at the domain wall, forming a closed loop. The resulting polarization arrangement corresponds to a stable Bloch-like skyrmion. Our original motivation was to verify whether a similar nanodomain can persist in the rhombohedral phase of  $\text{BaTiO}_3$ . The antiskyrmion reported here is such a stable nanodomain, but the geometry and topological charge of its polarization pattern is different from that of  $\text{PbTiO}_3$ . The peculiarity of this  $\text{BaTiO}_3$  nanodomain consists in its antiskyrmion nature.

*Topological and crystallographic considerations*—Both magnetic and electric skyrmions are string-like defects in a vector order parameter field. The nontrivial topology of the skyrmion is characterized by a nonzero skyrmion number  $N_{\text{sk}}$  given as an integral [18,25,26] of the topological density  $q(x, y) = (1/4\pi)\mathbf{u} \cdot (\partial_x \mathbf{u} \times \partial_y \mathbf{u})$  over the  $xy$  plane perpendicular to the skyrmion string, where  $\mathbf{u}$  is a unit vector field defining the direction of the order parameter. Topological charge with an invariant sign can be defined as  $Q = u_z(0) \cdot N_{\text{sk}}$ , where  $u_z(0)$  is the  $z$  component of the field direction vector in the core of the defect. This quantity  $Q$  is positive for skyrmions and negative for antiskyrmions (see Supplemental Material, note 2 [24]). In case of electric skyrmions the vector field  $\mathbf{u}$  is obtained from the local electric dipole of each unit cell and the discrete sum is used instead of the integral [17,18]. In particular, the  $\text{PbTiO}_3$  skyrmion shown in Fig. 1(a) yields its invariant topological charge of +1, common to Néel magnetic skyrmions in  $\text{GaV}_4\text{S}_8$  [27] or Bloch magnetic skyrmions in  $\text{MnSi}$  [1,4]. Here we report a stable nanodomain, carrying a topological charge of  $Q = -2$ .

\*Contact author: [hlinka@fzu.cz](mailto:hlinka@fzu.cz)

Published by the American Physical Society under the terms of the [Creative Commons Attribution 4.0 International license](https://creativecommons.org/licenses/by/4.0/). Further distribution of this work must maintain attribution to the author(s) and the published article's title, journal citation, and DOI.

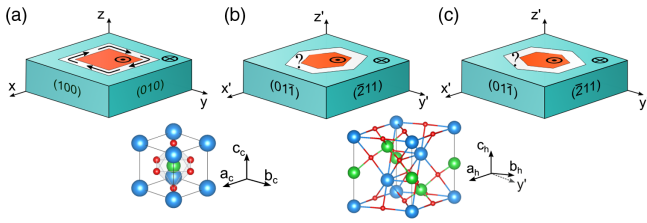


FIG. 1. Ultrasmall domains of antiparallel polarization in  $\text{PbTiO}_3$  and  $\text{BaTiO}_3$ . (a) Typical nanodomain configuration in tetragonal  $\text{PbTiO}_3$  as identified previously [17]. The polarization of the domain (orange) is parallel to the ferroelectric  $z$  axis, the outside (turquoise) has the opposite polarization. Black arrows in the wall region (white) represent the inner domain wall polarization, forming a loop. (b) The anticipated shape of a nanodomain within a rhombohedral  $\text{BaTiO}_3$  with the ferroelectric axis  $z' \parallel [111]$ . Domain walls are  $\{1\bar{1}0\}^*$  crystallographic planes, one of them is perpendicular to the  $x'$  axis. (c) Similar but with  $\{2\bar{1}1\}^*$  walls (one of them perpendicular to  $y'$  axis). Bottom left, respective orientation of the parent cubic perovskite cell with the lattice vectors  $a_c$ ,  $b_c$ , and  $c_c$ ; bottom right, the same structure redrawn in the hexagonal cell of rhombohedral  $\text{BaTiO}_3$  [ $a_h = (0, 1, \bar{1})$  and  $b_h = (\bar{1}, 0, 1)$  at  $120^\circ$ ]. Blue spheres stand for the Pb or Ba atoms, the green are the Ti atoms, red are the O atoms.

Plausible overall geometry of antiparallel nanodomains is sketched in Fig. 1. It follows from electrostatic considerations that domain boundaries should be parallel to the spontaneous ferroelectric polarization. The cross section of the nanodomain should agree with the macroscopic crystal symmetry of the ferroelectric domain itself and in case of strongly anisotropic domain wall energy it would be a polygon aligned with the crystallographic axes.

Let  $(x, y, z)$  be the Cartesian system for  $\text{PbTiO}_3$  and  $(x', y', z')$  refers to  $\text{BaTiO}_3$ . Crystallographic directions and planes are described with Miller indices  $h, k, l$  of the parent cubic structure. For the tetragonal ferroelectric  $\text{PbTiO}_3$ ,  $x \parallel [100]$  and the unique ferroelectric axis is  $z \parallel [001]$ , while in the rhombohedral phase of  $\text{BaTiO}_3$ ,  $x' \parallel [01\bar{1}]$ , and the unique ferroelectric axis is set as  $z' \parallel [111]$ . The brackets with an asterisk superscript ( $\{\}^*$ ) are used to denote the subset of planes equivalent within the symmetry of the given *ferroelectric domain* state (say, that of the core). For example, the  $\{100\}^*$  set for  $\text{PbTiO}_3$  domain with polarization along  $z$  contains only (100) and (010) planes. These low-index planes are those of  $\text{PbTiO}_3$  domain walls shown in Fig. 1(a). Similarly, the stable nanodomains in  $\text{BaTiO}_3$  should be delimited either by the set of  $\{1\bar{1}0\}^*$  facets or by the set of  $\{2\bar{1}\bar{1}\}^*$  facets. Both sets contain planes parallel to the ferroelectric axis  $z'$ . Using the convention of Ref. [28], we can state that  $\text{PbTiO}_3$  skyrmions are delimited by the neutral  $T180\{100\}$  walls (the  $\{100\}^*$ -oriented walls in Tetragonal phase corresponding to  $180^\circ$  rotation of the polarization), while the stable nanodomains in rhombohedral  $\text{BaTiO}_3$  are expected to be delimited by either  $R180\{1\bar{1}0\}$  domain walls [as in Fig. 1(b)] or by the  $R180\{2\bar{1}\bar{1}\}$  walls [as in Fig. 1(c)].

A necessary requirement for nonzero  $Q$  is a noncoplanar order parameter texture. The noncoplanarity of the polarization profile of the  $\text{PbTiO}_3$  nanodomain in Fig. 1(a) is related to the anticipated noncollinear structure of its  $T180\{100\}$  domain walls [29]. In  $\text{BaTiO}_3$ ,  $T180\{100\}$  domain walls are almost collinear but  $R180\{1\bar{1}0\}$  and  $R180\{2\bar{1}\bar{1}\}$  ones have a noncollinear character [28,30–32]. Thus, rhombohedral  $\text{BaTiO}_3$  also promises nontrivial topological defects.

*Computer experiment*—Since the properties of antiparallel domain walls of rhombohedral  $\text{BaTiO}_3$  are sensitive to the parametrization of the Ginzburg-Landau potential [31,32], we have employed here an *ab initio*-based atomistic shell model potential optimized for  $\text{BaTiO}_3$  molecular dynamics simulations [33,34]. This model has been successfully applied to reproduce various experimental data, including anomalous thermal diffuse scattering patterns [35] or short-range correlations in amorphous  $\text{BaTiO}_3$  [36]. Each atom is represented by core and shell, with its own position and charge. The potential energy includes pairwise short-range interactions as well as electrostatic Coulomb interactions (see Supplemental Material, note 3 [24]). Unless stated differently, we have used supercells made of  $12 \times 12 \times 4$  hexagonal unit cells (i.e., 8640 independent atoms) with periodic boundary conditions. Stable topological defects in the ferroelectric ground state were searched for through relaxing various initial configurations using standard atomistic optimization methods and classical molecular dynamics simulations at the temperature of 1 K (see Refs. [37,38] and Supplemental Material, note 4 [24]).

In order to avoid any bias towards the nonzero topological charge, our initial configurations were collinear ones. Within a homogeneously polarized supercell with  $P_{z'} < 0$  columnar region of hexagonal cross section, as in Fig. 1(b), was inverted. The inner diameter  $D$  of the hexagonal area of positive  $P_{z'}$  is given by  $D \approx N \cdot d$ , where  $d$  is the nominal spacing of the  $(1\bar{1}0)$  Ti planes in the parent cubic phase, and  $N$  is the dimensionless diameter of the hexagon.

*Resulting polarization texture*—The relaxed structure, obtained from the initially topologically trivial ( $Q = 0$ ) bubble nanodomain with  $N = 11$  and  $D \approx 3$  nm, is shown in Fig. 2(a). While the  $3m$  symmetry and the overall columnar shape persisted and the  $P_{z'}$  components did not change much, considerable in-plane polarization components developed spontaneously around the circumference of the nanodomain. Let us stress that the magnitude of the in-plane polarization is comparable to the value of the single-domain spontaneous polarization (see the labeling in Fig. 2(a) and Supplemental Material, note 5 [24]).

We note that also the radial and tangential *gradients* of the polarization are comparable so that the anticipated domain wall picture [Figs. 1(b) and 1(c)] does not apply: the width and the length of the individual wall segments are about the same. Instead, the texture forms a condensate of

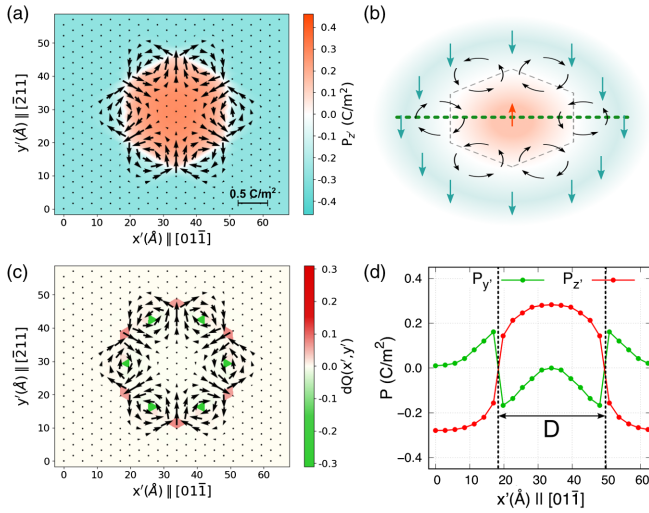


FIG. 2. A relaxed antiskyrmion nanodomain in BaTiO<sub>3</sub>. (a) Section through the  $N = 11$  antiskyrmion obtained by relaxation of a topologically trivial bubble nanodomain with the hexagonal section of Fig. 1(b). Local polarization calculated for each Ti site is projected along the  $z'$  axis. Non-negligible in-plane polarization components are marked by arrows, out of plane components are indicated by color. (b) Sketch of the pattern. The orange and turquoise arrows represent the nanodomain and the matrix. Curved arrows indicate the six vortices of in-plane polarization. (c) Topological charge density distribution  $q(x', y')dS$  superposed with the in-plane polarization. Values of  $q(x', y')dS$  are calculated for each individual triangular plaquette within the hexagonal sublattice of the projected Ti positions. (d) Transversal polarization components  $P_y, P_z$  along the green dashed line of panel (b) with indicated skyrmion size  $D$ . Note that the dominant, large negative- $Q$  contributions are located in the edges of the hexagon, that is, at the cores of the in-plane polarization vortices (shown by the green color).

six different vortices, with alternatively clockwise and anticlockwise rotation, each centered at one of the edges of the  $P_z > 0$  hexagon. Figure 2(b) shows the simplified sketch of the polarization arrangement.

Figure 2(c) shows the corresponding topological density, with six marked local minima in the vortex centers and six minor maxima near the vertices of the hexagon. Contributions of the elementary triangular plaquettes in the hexagonal lattice of the projected Ti positions correspond to the oriented solid angles subtended by the three dipoles in the corners of these plaquettes. None of the dipoles is zero and none of the plaquettes yields the corresponding solid angle critically close to the borderline value of  $2\pi$ . Therefore, summing up all these individual contributions, the total topological charge of  $Q = -2$  was obtained without any ambiguity.

*Stability of the electric antiskyrmion*—The relaxed configuration shown in Fig. 2 corresponds to the local energy minimum—its stability with respect to infinitesimal perturbations has been confirmed by checking the sign of all eigenvalues of the dynamical matrix corresponding to the

internal lattice degrees of freedom of the supercell (see Supplemental Material, note 6 [24]). We have also tested the stability with respect to the finite thermal fluctuations and confirmed that the molecular dynamics temperature can be safely risen to at least 20 K and the topological charge of  $-2$  is still preserved (see Supplemental Material, note 7 [24]). To further appreciate the robustness of the antiskyrmion configuration, we have also attempted to erase the nanodomain by a strong electric field aligned along the  $z'$  axis. It turned out that at 1 K the nanodomain is stable in a very broad range of  $-850 \text{ kV/cm} < E'_z < 1000 \text{ kV/cm}$ . In this range, the topological charge is always equal to  $-2$ . Since the critical fields are only 4–5 times less than the ideal coercive field limit for the homogeneous switching of the single domain state ( $E_c = 4600 \text{ kV/cm}$ ), we conclude that this electric antiskyrmion is a remarkably resistant object.

*Uniqueness of the antiskyrmion geometry*—We have attempted to vary the size of the initial topologically trivial nanodomains (see Fig. 3). The smallest resulting stable antiskyrmion had  $N = 9$  [see Fig. 3(b)]. For smaller initial diameters, the texture decays to the single domain state [see Fig. 3(a)]. For larger initial diameters, we could see modifications of the in-plane polarization pattern at the periphery of the antiskyrmion, induced by the interaction with its translational images generated by the periodic boundary conditions. This can lead to the  $3m > 3$  point group symmetry lowering (see Supplemental Material, note 8 [24]). These effects vanish when the periodic boundary box and therefore the antiskyrmion distances are large enough. Other initial geometries are shown in Fig. 4. For example, the initial domain with  $R180\{1\bar{1}0\}$  walls evolve to the same state as that starting with  $R180\{2\bar{1}\bar{1}\}$  walls [Figs. 2(a) and 4(a)]. On the other hand, the configuration similar to Fig. 2(a) but with inverted in-plane polarization is not stable [see Figs. 4(d)–4(f), note that flipping  $y'$  to  $-y'$  is not a symmetry operation of the parent phase]. Summarizing, there is only one type of stable columnar nanodomain solution for a given monodomain background.

*Mechanism*—It is worth noting that magnetic antiskyrmionic defects with  $Q < 0$  are known [39], and they can even be derived from the canonical Bogdanov-Yablonskii phenomenological theory [40,41]. Nevertheless, the parent paraelectric phase of BaTiO<sub>3</sub> is centrosymmetric, so the formal ferroelectric analogue [42] of the bulk Dzialoshinskii-Moriya interaction is forbidden. Therefore, the Bogdanov-Yablonskii theory [40] does not explain the existence of the antiskyrmions investigated in this work, and we can also exclude the interfacial Dzialoshinskii-Moriya mechanism [43] since there is no interface in our simulations. Likewise, the Bloch wall scenario of bulk skyrmions in PbTiO<sub>3</sub> does not apply here, because the BaTiO<sub>3</sub> antiskyrmion is not composed of Bloch walls—e.g., the  $P_y(x')$  path in Fig. 2(d) is that of the so-called bichiral wall [44–46].

So why the BaTiO<sub>3</sub> nanodomains have  $Q = -2$  instead of  $Q = 1$  as in PbTiO<sub>3</sub>? The stability of the

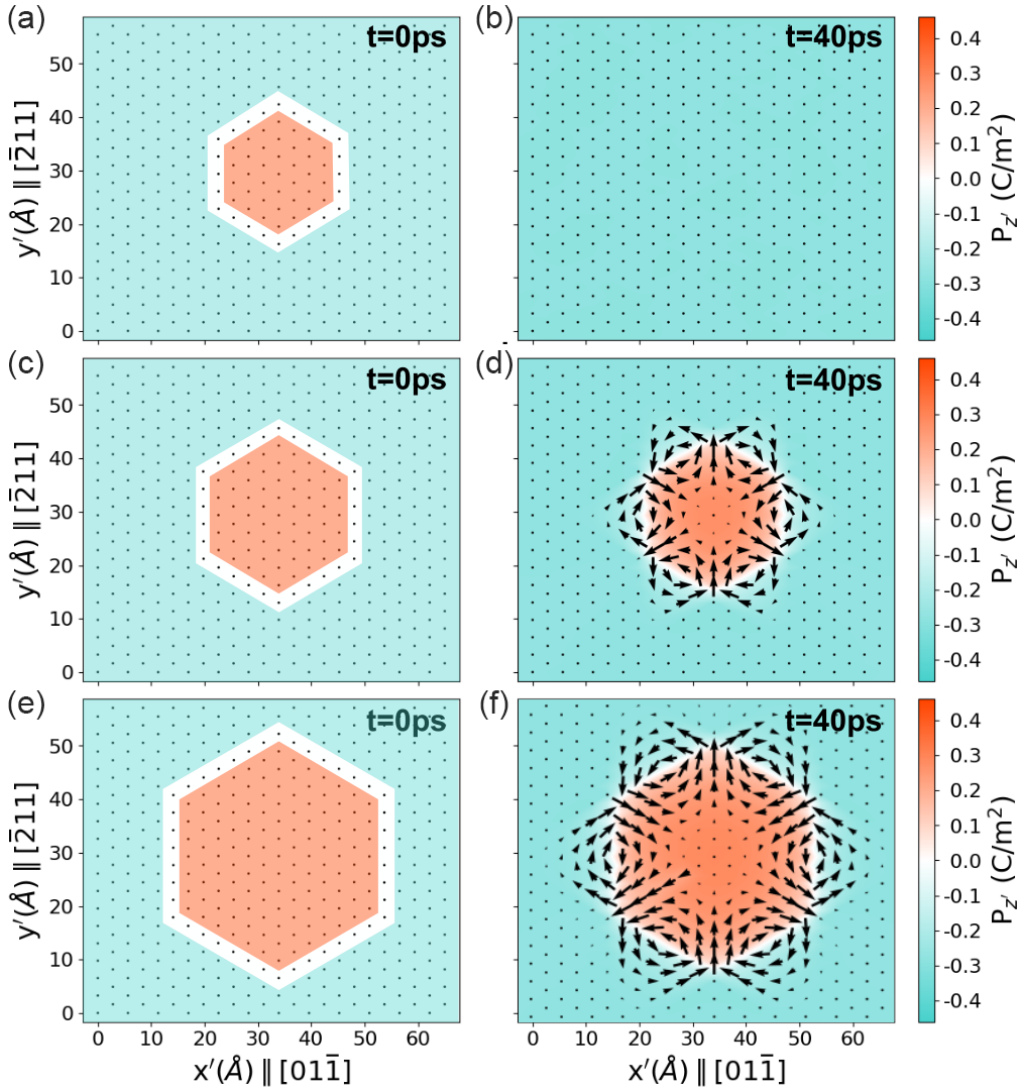


FIG. 3. Formation of antiskyrmions with different sizes. Left panels (a),(c),(e) show the initial nanodomain with a topologically trivial colinear polarization configuration. From top to bottom, the size parameter is  $N = 7$ ,  $N = 9$ , and  $N = 13$ . Right panels (b),(d),(f) show the respective relaxed configuration after 40 ps of MD relaxation at  $T = 1$  K. For  $N = 13$ , a larger periodic box with  $16 \times 16 \times 4$  hexagonal unit cells is used.

antiskyrmion configurations in  $\text{BaTiO}_3$  is favored by a combination of a moderate anisotropy of the anharmonicity of the parent phase electric susceptibility with a pronounced anisotropy of the polarization correlations. These two aspects, manifested in peculiar diffuse scattering patterns [35] and highly anisotropic soft phonon dispersion relations [47], imply that (i) the local polarizations are close to one the 8 possible  $\langle 111 \rangle$  directions, and (ii) polarization directions of the nearest neighbor sites, projected along the common Ti—O—Ti bond, are strongly correlated (8-site model) [35,48,49]. Another consequence is that the R180 domain walls have an order of magnitude higher energies than the R71 domain walls [28,30].

In this context, it is instructive to idealize the stable antiskyrmion structure by tilting each local polarization to its nearest  $\langle 111 \rangle$ -type direction. Then, one can see all R180

walls are split in three R71 domain walls (see Supplemental Material, note 9 [24]): the  $P_z > 0$  hexagon is formed by mechanically compatible  $R71\{01\bar{1}\}^*$ -walls, the other R71-walls form the outline of the vortices, and the central radial sections through the vortices are formed by  $R109\{\bar{2}11\}^*$ -walls (see Supplemental Material, note 9 [24]). Note that strictly parallel layout of these three *distinct* R71 domain walls would be prohibitive due to the strong depolarization field, while the sequence of flux closure vortices arranged on a curved cylindrical surface allows to circumvent the electrostatic problem.

Summarizing, the formation of the antiskyrmion represents a decay of a curved R180 domain wall into energetically more favorable R71 domain wall triplets. The key ingredient favoring R71 against R180 walls is the  $G_{1111} - G_{1122} \gg G_{1212}$  anisotropy of the correlation energy [28]

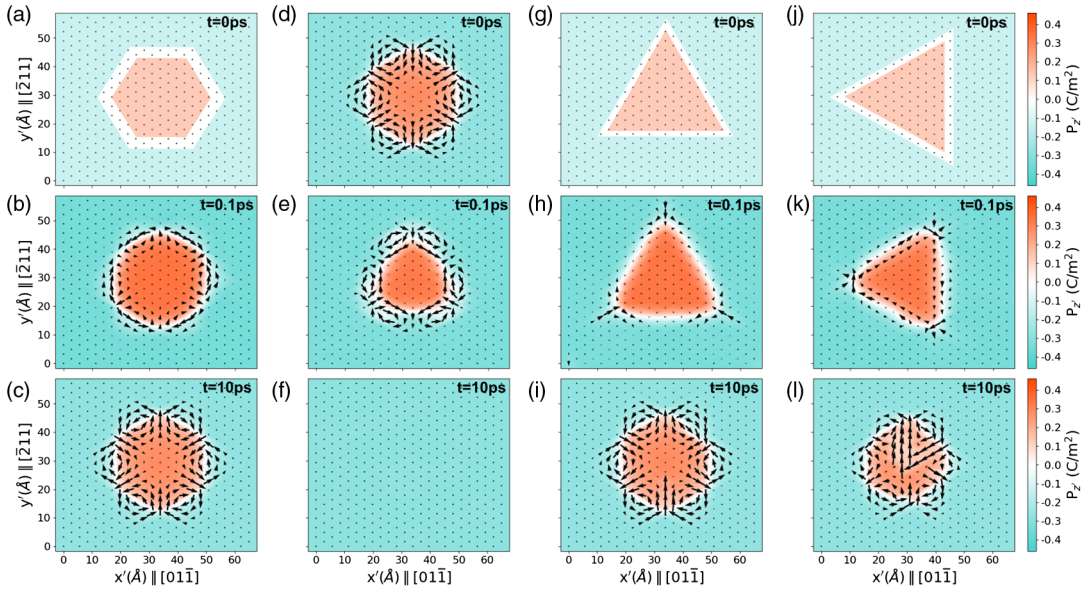


FIG. 4. Decay of alternative initial configurations. Top panels show the initial configurations, middle panels show structures after 0.1 ps of MD evolution and bottom panels show the close to final equilibrium configurations registered after 10 ps of MD evolution. Panels (a),(b),(c)—configuration with  $R180\{\bar{2}11\}$  domain walls transforms to that with  $R180\{0\bar{1}\bar{1}\}$  domain walls. Panels (d),(e),(f)—configuration similar to Fig. 2(a) but with inverted in-plane polarization decays into the single domain. Panels (g),(h),(i) and (j),(k),(l) show evolutions from configurations with  $R180\{\bar{2}11\}$  and  $R180\{0\bar{1}\bar{1}\}$  domain walls, respectively.

$G_{ijkl}dP_i/dx_jdP_k/dx_l$  which is typical for  $BaTiO_3$  and  $KNbO_3$  but absent in  $PbTiO_3$ . To validate this mechanism, we have applied the same computational methodology to  $PbTiO_3$  and  $KNbO_3$  as well. Indeed, in  $PbTiO_3$  the Bloch skyrmion forms, while in  $KNbO_3$ , the  $Q = -2$  antiskyrmion is found (see Supplemental Material, note 10 [24]).

*Final remarks*—While we are not aware of any investigations of a similar electric antiskyrmion defects, the higher-skyrmion number  $|Q| > 1$  has been already considered for magnetic systems [49–53]. The geometrically close textures are the  $Q = -2$  magnetic textures of hexagonal (also called triangular) magnets [50,51] and ultrathin magnetic films [54,55]. One of the remarkable common aspects of these magnetic and electric antiskyrmions that deserves more attention is the concentration of the  $dQ$  in a few “hot spots” with fractional topological charge [18,50,56]. In the present antiskyrmion, there are six such hot spots, each carrying topological charge of about  $Q \approx -1/3$ . These “quarklike” hot spots are located at the frustrated triangular plaquettes at the crossings of the tangential R71 and radial R109 walls. Considering that the mirror symmetry planes divide the antiskyrmion into six equivalent parts, it implies that the total topological charge is roughly  $Q \approx -2$  and, since it has to be an integer, it is exactly  $Q = -2$ .

Present results are based on a fully atomistic model (see Refs. [33,34,37,38]). We hope that follow up studies with a more simplified models will allow to address the mutual antiskyrmion interactions and the emerging chirality (Supplemental Material, note S8 [24]) reminding chiral states of spatially confined ferroelectric dots [57,58].

More rigorous density functional calculation of the entire antiskyrmion is also beyond our possibilities, but using the available methodology [59,60], we have conducted first-principle optimization of dense planar Bloch and bichiral  $R180\{110\}$  domain wall sets. Comparison with the corresponding optimized shell-model polarization profiles supports the adopted  $BaTiO_3$  shell model (see Supplemental Material, note 11 [24]).

In summary, we realized that the ferroelectric nanodomains with a miniscule 2–3 nm diameter can be stabilized at zero field in  $BaTiO_3$  and that these nanodomains have a characteristic hexagonal shape. We have found that six vortices develop, each on one facet of the nanodomain, and each carry a fractional topological charge of  $-1/3$ , giving altogether the unusual net skyrmion topological charge of  $-2$ . We computationally affirmed the stability of these qualitatively novel nanoscale topological defects, their remarkable resilience to the electric field and explored the kinetics of their formation.

*Acknowledgments*—This work was supported by the Czech Science Foundation (Project No. 19-28594X).

- [1] S. Mühlbauer, B. Binz, F. Jonietz, C. Pfleiderer, A. Rosch, A. Neubauer, R. Georgii, and P. Böni, Skyrmion lattice in a chiral magnet, *Science* **323**, 915 (2009).
- [2] U. K. Röbber, A. N. Bogdanov, and C. Pfleiderer, Spontaneous skyrmion ground states in magnetic metals, *Nature (London)* **442**, 797 (2006).

- [3] A. Fert, N. Reyren, and V. Cros, Magnetic skyrmions: Advances in physics and potential applications, *Nat. Rev. Mater.* **2**, 17031 (2017).
- [4] A. Neubauer, C. Pfleiderer, B. Binz, A. Rosch, R. Ritz, P. G. Niklowitz, and P. Böni, Topological Hall effect in the A phase of MnSi, *Phys. Rev. Lett.* **102**, 186602 (2009).
- [5] T. Schulz, R. Ritz, A. Bauer, M. Halder, M. Wagner, C. Franz, C. Pfleiderer, K. Everschor, M. Garst, and A. Rosch, Emergent electrodynamics of skyrmions in a chiral magnet, *Nat. Phys.* **8**, 301 (2012).
- [6] P. Bruno, V. K. Dugaev, and M. Taillefumier, Topological Hall effect and Berry phase in magnetic nanostructures, *Phys. Rev. Lett.* **93**, 096806 (2004).
- [7] J. Zang, M. Mostovoy, J. H. Han, and N. Nagaosa, Dynamics of skyrmion crystals in metallic thin films, *Phys. Rev. Lett.* **107**, 136804 (2011).
- [8] K. Litzius, I. Lemesh, B. Krüger, P. Bassirian, L. Caretta, K. Richter, F. Büttner, K. Sato, O. A. Tretiakov, J. Förster, R. M. Reeve, M. Weigand, I. Bykova, H. Stoll, G. Schütz, G. S. D. Beach, and M. Kläui, Skyrmion Hall effect revealed by direct time-resolved X-ray microscopy, *Nat. Phys.* **13**, 170 (2017).
- [9] W. Jiang, X. Zhang, G. Yu, W. Zhang, X. Wang, M. B. Jungfleisch, J. E. Pearson, X. Cheng, O. Heinonen, K. L. Wang, Y. Zhou, A. Hoffmann, and S. G. E. te Velthuis, Direct observation of the skyrmion Hall effect, *Nat. Phys.* **13**, 162 (2017).
- [10] Y. Fujishiro, N. Kanazawa, T. Nakajima, X. Z. Yu, K. Ohishi, Y. Kawamura, K. Kakurai, T. Arima, H. Mitamura, A. Miyake, K. Akiba, M. Tokunaga, A. Matsuo, K. Kindo, T. Koretsune, R. Arita, and Y. Tokura, Topological transitions among skyrmion- and hedgehog-lattice states in cubic chiral magnets, *Nat. Commun.* **10**, 1059 (2019).
- [11] N. Kent, N. Reynolds, D. Raftrey, I. T. G. Campbell, S. Virasawmy, S. Dhuey, R. V. Chopdekar, A. Hierro-Rodriguez, A. Sorrentino, E. Pereiro, S. Ferrer, F. Hellman, P. Sutcliffe, and P. Fischer, Creation and observation of Hopfions in magnetic multilayer systems, *Nat. Commun.* **12**, 1562 (2021).
- [12] S. Zhang, F. Kronast, G. van der Laan, and T. Hesjedal, Real-space observation of skyrmionium in a ferromagnet-magnetic topological insulator heterostructure, *Nano Lett.* **18**, 1057 (2018).
- [13] M. Finazzi, M. Savoini, A. R. Khorsand, A. Tsukamoto, A. Itoh, L. Duò, A. Kirilyuk, Th. Rasing, and M. Ezawa, Laser-induced magnetic nanostructures with tunable topological properties, *Phys. Rev. Lett.* **110**, 177205 (2013).
- [14] J. Barker and O. A. Tretiakov, Static and dynamical properties of antiferromagnetic skyrmions in the presence of applied current and temperature, *Phys. Rev. Lett.* **116**, 147203 (2016).
- [15] C. Back, V. Cros, H. Ebert, K. Everschor-Sitte, A. Fert, M. Garst, Tianping Ma, S. Mankovsky, T. L. Monchesky, M. Mostovoy, N. Nagaosa, S. S. P. Parkin, C. Pfleiderer, N. Reyren, A. Rosch, Y. Taguchi, Y. Tokura, K. von Bergmann, and J. Zang, The 2020 skyrmionics roadmap, *J. Phys. D* **53**, 363001 (2020).
- [16] S. Das *et al.*, Observation of room-temperature polar skyrmions, *Nature (London)* **568**, 368 (2019).
- [17] M. A. P. Gonçalves, C. Escorihuela-Sayalero, P. Garca-Fernández, J. Junquera, and J. Íñiguez, Theoretical guidelines to create and tune electric skyrmion bubbles, *Sci. Adv.* **5**, eaau7023 (2019).
- [18] Y. Nahas, S. Prokhorenko, L. Louis, Z. Gui, I. Kornev, and L. Bellaiche, Discovery of stable skyrmionic state in ferroelectric nanocomposites, *Nat. Commun.* **6**, 8542 (2015).
- [19] S. Das *et al.*, Local negative permittivity and topological phase transition in polar skyrmions, *Nat. Mater.* **20**, 194 (2021).
- [20] R. Zhu *et al.*, Dynamics of polar skyrmion bubbles under electric fields, *Phys. Rev. Lett.* **129**, 107601 (2022).
- [21] K. T. Kim *et al.*, Chiral structures of electric polarization vectors quantified by X-ray resonant scattering, *Nat. Commun.* **13**, 1769 (2022).
- [22] Y.-T. Shao, S. Das, Z. Hong, R. Xu, S. Chandrika, F. Gómez-Ortiz, P. García-Fernández, L.-Q. Chen, H. Y. Hwang, J. Junquera, L. W. Martin, R. Ramesh, and D. A. Muller, Emergent chirality in a polar meron to skyrmion phase transition, [arXiv:2101.04545](https://arxiv.org/abs/2101.04545).
- [23] P. Shafer, P. García-Fernández, P. Aguado-Puente, A. R. Damodaran, A. K. Yadav, C. T. Nelson, S.-L. Hsu, J. C. Wojdeł, J. Íñiguez, L. W. Martin, E. Arenholz, J. Junquera, and R. Ramesh, Emergent chirality in the electric polarization texture of titanate superlattices, *Proc. Natl. Acad. Sci. U.S.A.* **115**, 915 (2018).
- [24] See Supplemental Material at <http://link.aps.org/supplemental/10.1103/PhysRevLett.133.066802> for more information about the terminological issues (note 1), invariant sign of the skyrmion topological charge (note 2), description of the model (note 3), computational details (note 4), histograms of atomic displacement sizes (note 5), small displacement stability (note 6), stability vs temperature fluctuations (Suppl. note 7), sensitivity to the size of the simulation box (note 8), antiskyrmion geometry elaboration and decay of R180 domain walls (note 9), nano-domains in lead titanate and potassium niobate (note 10), and auxiliary comparison of shell model and DFT calculations of a dense system of planar R180 domain walls (note 11).
- [25] S. Seki and M. Mochizuki, *Skyrmions in Magnetic Materials* (Springer International Publishing, New York, 2016).
- [26] N. Nagaosa and Y. Tokura, Topological properties and dynamics of magnetic skyrmions, *Nat. Nanotechnol.* **8**, 899 (2013).
- [27] I. Kézsmárki, S. Bordács, P. Milde, E. Neuber, L. M. Eng, J. S. White, H. M. Rønnow, C. D. Dewhurst, M. Mochizuki, K. Yanai, H. Nakamura, D. Ehlers, V. Tsurkan, and A. Loidl, Néel-type skyrmion lattice with confined orientation in the polar magnetic semiconductor GaV<sub>4</sub>S<sub>8</sub>, *Nat. Mater.* **14**, 1116 (2015).
- [28] P. Marton, I. Rychetsky, and J. Hlinka, Domain walls of ferroelectric BaTiO<sub>3</sub> within the Ginzburg-Landau-Devonshire phenomenological model, *Phys. Rev. B* **81**, 144125 (2010).
- [29] J. C. Wojdeł and J. Íñiguez, Ferroelectric transitions at ferroelectric domain walls found from first principles, *Phys. Rev. Lett.* **112**, 247603 (2014).

- [30] M. Taherinejad, D. Vanderbilt, P. Marton, V. Stepkova, and J. Hlinka, Bloch-type domain walls in rhombohedral BaTiO<sub>3</sub>, *Phys. Rev. B* **86**, 155138 (2012).
- [31] V. Stepkova, P. Marton, and J. Hlinka, Stress-induced phase transition in ferroelectric domain walls of BaTiO<sub>3</sub>, *J. Phys. Condens. Matter* **24**, 212201 (2012).
- [32] J. Hlinka, V. Stepkova, P. Marton, and P. Ondrejko, *Topological Structures in Ferroic Materials*, edited by J. Seidel (Springer, Switzerland, 2016), pp. 161–180.
- [33] S. Tinte, M. G. Stachiotti, S. R. Phillpot, M. Sepiarsky, D. Wolf, and R. L. Migoni, Ferroelectric properties of Ba<sub>x</sub>Sr<sub>1-x</sub>TiO<sub>3</sub> solid solutions obtained by molecular dynamics simulation, *J. Phys. Condens. Matter* **16**, 3495 (2004).
- [34] M. Sepiarsky, A. Asthagiri, S. R. Phillpot, M. G. Stachiotti, and R. L. Migoni, Atomic-level simulation of ferroelectricity in oxide materials, *Curr. Opin. Solid State Mater. Sci.* **9**, 107 (2005).
- [35] M. Paściak, T. R. Welberry, J. Kulda, S. Leoni, and J. Hlinka, Dynamic displacement disorder of cubic BaTiO<sub>3</sub>, *Phys. Rev. Lett.* **120**, 167601 (2018).
- [36] T. Hashimoto and H. Moriwake, Structure of amorphous BaTiO<sub>3</sub> by molecular dynamics simulations using a shell model, *Physica (Amsterdam)* **579B**, 411799 (2020).
- [37] I. T. Todorov, W. Smith, K. Trachenko, and M. T. Dove, DL POLY 3: New dimensions in molecular dynamics simulations via massive parallelism, *J. Mater. Chem.* **16**, 1911 (2006).
- [38] J. D. Gale and A. L. Rohl, The General Utility Lattice Program (GULP), *Mol. Simul.* **29**, 291 (2003).
- [39] A. K. Nayak, V. Kumar, T. Ma, P. Werner, E. Pippel, R. Sahoo, F. Damay, U. K. Röbler, C. Felser, and S. S. P. Parkin, Magnetic antiskyrmions above room temperature in tetragonal Heusler materials, *Nature (London)* **548**, 561 (2017).
- [40] A. N. Bogdanov and D. A. Yablonskii, Thermodynamically stable “vortices” in magnetically ordered crystals. The mixed state of magnets, *Zh. Eksp. Teor. Fiz.* **95**, 178 (1989).
- [41] A. N. Bogdanov and C. Panagopoulos, Physical foundations and basic properties of magnetic skyrmions, *Nat. Rev. Phys.* **2**, 492 (2020).
- [42] K. C. Erb and J. Hlinka, Vector, bidirector, and Bloch skyrmion phases induced by structural crystallographic symmetry breaking, *Phys. Rev. B* **102**, 024110 (2020).
- [43] M. Hoffmann, B. Zimmermann, G. P. Müller, D. Schürhoff, N. S. Kiselev, C. Melcher, and S. Blügel, Antiskyrmions stabilized at interfaces by anisotropic Dzyaloshinskii-Moriya interactions, *Nat. Commun.* **8**, 308 (2017).
- [44] B. Houchmandzadeh, J. Lajzerowicz, and E. Salje, Order parameter coupling and chirality of domain walls, *J. Phys. Condens. Matter* **3**, 5163 (1991).
- [45] P. V. Yudin, A. K. Tagantsev, E. A. Eliseev, A. N. Morozovska, and N. Setter, Bichiral structure of ferroelectric domain walls driven by flexoelectricity, *Phys. Rev. B* **86**, 134102 (2012).
- [46] P. V. Yudin, A. K. Tagantsev, and N. Setter, Bistability of ferroelectric domain walls: Morphotropic boundary and strain effects, *Phys. Rev. B* **88**, 024102 (2013).
- [47] J. Harada, J. D. Axe, and G. Shirane, Neutron-scattering study of soft modes in cubic BaTiO<sub>3</sub>, *Phys. Rev. B* **4**, 155 (1971).
- [48] R. Comes, M. Lambert, and A. Guinier, The chain structure of BaTiO<sub>3</sub> and KNbO<sub>3</sub>, *Solid State Commun.* **6**, 715 (1968).
- [49] N. Mohanta and E. Dagotto, Interfacial phase frustration stabilizes unconventional skyrmion crystals, *npj Quantum Mater.* **7**, 76 (2022).
- [50] D. Amoroso, P. Barone, and S. Picozzi, Spontaneous skyrmionic lattice from anisotropic symmetric exchange in a Ni-halide monolayer, *Nat. Commun.* **11**, 5784 (2020).
- [51] R. Ozawa, S. Hayami, and Y. Motome, Zero-field skyrmions with a high topological number in itinerant magnets, *Phys. Rev. Lett.* **118**, 147205 (2017).
- [52] A. O. Leonov and M. Mostovoy, Multiply periodic states and isolated skyrmions in an anisotropic frustrated magnet, *Nat. Commun.* **6**, 8275 (2015).
- [53] M. N. Potkina, I. S. Lobanov, O. A. Tretiakov, H. Jónsson, and V. M. Uzdin, Stability of long-lived antiskyrmions in the Mn-Pt-Sn tetragonal Heusler material, *Phys. Rev. B* **102**, 134430 (2020).
- [54] B. Dupé, C. N. Kruse, T. Dornheim, and S. Heinze, How to reveal metastable skyrmionic spin structures by spin-polarized scanning tunneling microscopy, *New J. Phys.* **18**, 055015 (2016).
- [55] S. Heinze, K. von Bergmann, M. Menzel, J. Brede, A. Kubetzka, R. Wiesendanger, G. Bihlmayer, and S. Blügel, Spontaneous atomic-scale magnetic skyrmion lattice in two dimensions, *Nat. Phys.* **7**, 713 (2011).
- [56] S. Z. Lin, A. Saxena, and C. D. Batista, Skyrmion fractionalization and merons in chiral magnets with easy-plane anisotropy, *Phys. Rev. B* **91**, 224407 (2015).
- [57] Yu. Tikhonov, S. Kondovych, J. Mangeri, M. Pavlenko, L. Baudry, A. Sené, A. Galda, S. Nakhmanson, O. Heinonen, A. Razumnaya, I. Luk’yanchuk, and V. M. Vinokur, Controllable skyrmion chirality in ferroelectrics, *Sci. Rep.* **10**, 8657 (2020).
- [58] V. Stepkova, P. Marton, N. Setter, and J. Hlinka, Closed-circuit domain quadruplets in BaTiO<sub>3</sub> nanorods embedded in a SrTiO<sub>3</sub> film, *Phys. Rev. B* **89**, 060101(R) (2014).
- [59] J. M. Soler, E. Artacho, J. D. Gale, A. García, J. Junquera, P. Ordejón, and D. Sánchez-Portal, The SIESTA method for *ab initio* order-N materials simulation, *J. Phys. Condens. Matter* **14**, 2745 (2002).
- [60] Z. Wu and R. E. Cohen, More accurate generalized gradient approximation for solids, *Phys. Rev. B* **73**, 235116 (2006).